GPS Solutions (2018) 22:79
https://doi.org/10.1007/s10291-018-0746-6

ORIGINAL ARTICLE

# Reduced dynamic and kinematic precise orbit determination for the Swarm mission from 4 years of GPS tracking

**Oliver Montenbruck**[1] · **Stefan Hackel**[1] · **Jose van den Ijssel**[2] · **Daniel Arnold**[3]

Received: 10 April 2018 / Accepted: 12 June 2018 / Published online: 15 June 2018


**Abstract**
Precise science orbits for the first 4 years of the Swarm mission have been generated from onboard GPS measurements in a systematic reprocessing using refined models and processing techniques. Key enhancements relate to the introduction of macro-models for a more elaborate non-gravitational force modeling (solar radiation pressure, atmospheric drag and lift, earth albedo), as well as carrier phase ambiguity fixing. Validation using satellite laser ranging demonstrates a 30% improvement in the precision of the reduced dynamic orbits with resulting errors at the 0.5–1 cm level (1D RMS). A notable performance improvement is likewise achieved for the kinematic orbits, which benefit most from the ambiguity fixing and show a 50% error reduction in terms of SLR residuals while differences with respect to reduced dynamic ephemerides amount to only 1.7 cm (median of daily 3D RMS). Compared to the past kinematic science orbits based on float-ambiguity estimates, the new kinematic position solutions exhibit a factor of reduction of two to three in Allan deviation at time scales of 1000s and higher, and promise an improved recovery of low-degree and -order gravity field coefficients in Swarm gravity field analyses.

**Keywords** POD · GPS · SLR · Ambiguity fixing · Non-gravitational forces

## Introduction

Swarm is a small-satellite "Earth Explorer" mission of the European Space Agency (ESA) dedicated to the exploration of the earth's magnetic field (Friis-Christensen et al. 2008; Olsen et al. 2016). Further science objectives include investigations of the earth's atmosphere (Siemes et al. 2016) and gravity field (Jäggi et al. 2016; da Encarnação et al. 2016). The Swarm constellation is made up of three identical spacecraft. These satellites orbit the earth in polar orbits with an 87° inclination and initial altitudes of about 470 km (Swarm-A, -C) and 520 km (Swarm-B). While the Swarm-A/C satellites remain close to each other with mutual separations of about 50–200 km, Swarm-B exhibits a different orbital period and its orbital plane drifts relative to that of the Swarm-A/C pair by about 25° per year (Sieg and Diekmann 2016).

Key payloads of each Swarm satellite include an absolute scalar magnetometer and a vector field magnetometer, the Langmuir probe and the thermal ion imager for measuring the electric field, a set of accelerometers, and star cameras. The spacecraft are, furthermore, equipped with a dual frequency GPS receiver (Zangerl et al. 2014) for precise orbit determination and onboard navigation. GPS observations and the derived orbit determination support the geocoding of other instrument data, but likewise contribute to ionospheric research, thermospheric density determination, and gravity field recovery.

Kinematic and reduced dynamic precise science orbits (PSOs) are generated by TU Delft for the ESA on a routine basis (van den IJssel et al. 2015) using the GNSS High-precision Orbit determination Software Tools (GHOST; Wermuth et al. 2010). Over the 4 years of operations conducted so far, Swarm GPS tracking—and, in consequence, the orbit

✉ Oliver Montenbruck
oliver.montenbruck@dlr.de

Stefan Hackel
stefan.hackel@dlr.de

Jose van den Ijssel
J.A.A.vandenIJssel@tudelft.nl

Daniel Arnold
daniel.arnold@aiub.unibe.ch

[1] Deutsches Zentrum für Luft- und Raumfahrt, German Space Operations Center, 82234 Weßling, Germany

[2] TU Delft, Kluyverweg 1, 2629 HS Delft, The Netherlands

[3] AIUB, Sidlerstrasse 5, 3012 Bern, Switzerland

determination quality—have continuously improved through receiver configuration changes (van den IJssel et al. 2016; Dahle et al. 2017) and an overall decrease in ionospheric scintillation activity between 2013 and 2017.

Carrier phase measurements of the Swarm GPS receivers have traditionally suffered from half-cycle ambiguities, which prevent or notably hamper ambiguity resolution in GPS-based precise orbit determination. More recently, this limitation could be overcome through an enhanced approach for building carrier phase measurements out of raw correlator outputs of the given receiver type, which takes into account the navigation data bit sign and the properties of the semi-codeless P(Y)-code tracking of the Swarm GPS receiver (Montenbruck et al. 2017). A reprocessing of GPS raw data from the Swarm-A/B/C satellites covering the period from launch (Nov. 22, 2013) to end of 2017 was, therefore, performed for this study to obtain observation files in the receiver independent exchange format (RINEX) that support integer ambiguity resolution.

Following an overview of the employed models and processing strategies for precise orbit determination (POD) in the new and heritage science orbit generation, we discuss the achieved performance improvements based on the analysis of satellite laser ranging (SLR) residuals. The quality of kinematic orbits is, furthermore, assessed in terms of ephemeris comparisons and through the position Allan deviation as a measure for the smoothness and coherence of the solutions over different time scales.

## POD processing and models

An overview of processing models used for the initial version of precise science orbits (van den IJssel et al. 2015) and in the present reprocessing is given in Table 1. Within each processing chain, the same data and observation models are used for the respective kinematic and reduced dynamic orbit determination.

**Table 1** Processing standards for original and reprocessed precise science orbits of the Swarm satellites

| Original PSOs | Reprocessing |
|---|---|
| GPS observation model | |
| Undifferenced ionosphere-free code and carrier phase combinations | Same |
| 1 s sampling | 5 s sampling |
| CODE final orbits and 5 s clocks | GRG orbits and 30 s clocks, densified to 5 s using CODE clocks; GRG wide-lane bias product |
| igs08.atx(up to Jan 2017)/igs14.atx models of GPS transmit antenna phase center offset and variations | Same |
| Receiver antenna phase center offset from operator supplied center-of-mass position, antenna position and star camera spacecraft attitude; inflight calibrated receiver antenna phase patterns | Same |
| Carrier phase wind-up | Same |
| ICRF-to-IGB08/IGS114 reference transformation based on IERS1996 conventions and IGS earth orientation parameters | Same |
| Reduced dynamic orbit model | |
| GOCO03S earth gravity field model (100×100), linear time variation of $C_{20}$, $C_{21}$, $S_{21}$; luni-solar perturbations (analytical series); solid earth and pole tides (IERS2003); ocean tides; post-Newtonian corrections | Same |
| Cannon-ball model for solar radiation pressure and atmospheric drag, Jachhia-71 density model | Macro-model (15 plates) for solar radiation pressure, earth albedo and infrared radiation, and atmospheric drag and lift; NRLMSIS-00 density and composition model |
| Thrust arcs (maneuvers); piecewise constant empirical accelerations at 10-min intervals | Same |
| Estimation | |
| Batch least-squares | Same |
| Epoch wise clock offsets | Same |
| Kinematic POD: epoch-wise positions | Same |
| Reduced dynamic POD: epoch state vector, scale factors for solar radiation pressure and atmospheric forces, maneuvers and empirical acceleration | Same; fixed scale factor for earth radiation pressure |
| Float-valued carrier phase ambiguities | Pass-by-pass wide-lane and L1 carrier phase ambiguity fixing |

An undifferenced processing concept is adopted, in which the GPS orbits and clock offsets are fixed to a priori values as given in the respective products of the International GNSS Service (IGS; Johnston et al. 2017) and its analysis centers. More specifically, data products of the Center for Orbit Determination in Europe (CODE; Dach et al. 2017) were used for the legacy PSO generation, while "GRG (Groupe de Recherche de Géodésie Spatiale)" products (Loyer et al. 2012) of the CNES/CLS (Centre National d'Études Spatiales/Collecte Localisation Satellites) analysis center were employed for the present reprocessing. The GRG products are specifically designed to support single-receiver ambiguity fixing by providing wide-lane ambiguities and clock offset solutions that incorporate fractional L1 phase biases.

To facilitate processing of GPS observations at measurement intervals below the 30 s sampling of standard IGS clock products, dedicated high-rate solutions of the GPS satellite clock offsets are required. Use of such products helps to avoid, or at least minimize, noise contributions from clock offset interpolation. Precise GPS clock information at the native measurement interval is particularly desirable for purely kinematic POD which suffers most from clock interpolation errors. Starting with the GOCE mission, GPS clock solution with sampling intervals down to 1 s have, therefore, been generated at CODE (Bock et al. 2009).

A 5 s CODE clock product is presently made available to the public and was used by TU Delft for the Swarm PSO generation from the very beginning of the mission. GRG clock products, in contrast, are only available at 30 s intervals and were, therefore, blended with 5 s CODE clock products as illustrated in Fig. 1. At each 5 s epoch, the difference between CODE 5 s clocks offsets and the interpolated values across the adjacent 30 s grid points is first determined and then added to the interpolated clock offset from 30 s GRG data at the same epoch. In this way, a merged clock offset product at 5 s grid resolution is obtained, that retains the system time scale and fractional phase biases of the GRG clock product, but properly reflects all short-term variations of the GPS satellite clocks. The benefit of the blended 5 s clock product over the original GRG 30 s product depends on the short-term stability of the atomic frequency standard and is most pronounced for GPS satellites operated with a cesium clock. Overall, use of the blended GRG/CODE clocks enables a notable reduction of the measurement residuals when processing observations with a 5 s sampling interval. By way of example, Swarm-B carrier phase residuals of the ambiguity-fixed POD solution on day of year 2017/300 were reduced from 6.9 to 5.0 mm when replacing the GRG 30 s clock product with the blended high-rate clock product.

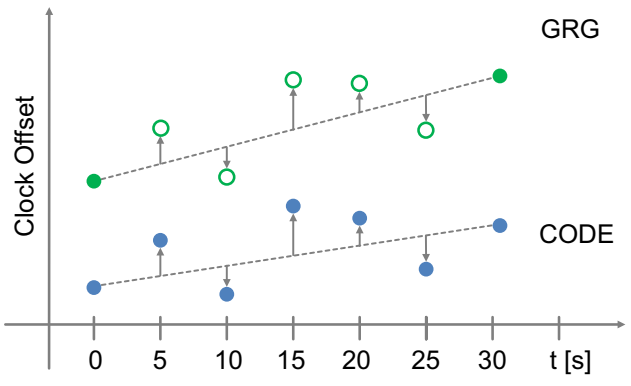


**Fig. 1** Generation of high-rate GRG satellite clock offsets through blending with 5 s CODE clock offset

Given the non-availability of precise 1 Hz clock products, a reduced 5 s sampling of the GPS observations has been employed for the reprocessing to model carrier phase observations with the highest possible precision. Subject to a compatible weighting of observations and a priori constraints for other estimation parameters, no benefit of 1 Hz sampling rates could be observed for the reduced dynamic orbit solutions that would justify the increased processing. For kinematic orbits, the reduced 5 s observation sampling is directly reflected in a sparser set of position solutions. However, the resulting spacing of about 40 km or less than 0.5° in along-track direction is still compatible with common user needs for these products in gravity field estimation.

With respect to non-gravitational forces, the cannon-ball models used for generation of the PSO have been replaced by a 15-plate macro-model for the boom and main body (see Fig. 2; Table 2). Optical properties for each plate comprise the effective fraction of absorbed ($\alpha$), diffusely reflected ($\delta$), and specularly reflected ($\rho$) photons in the visual (vis) and infrared (IR) regime for the given material mix based on data provided by the spacecraft manufacturer. Following Cerri et al. (2010), the solar and earth radiation pressure (SRP, ERP) models takes into account spontaneous re-emission of absorbed radiation for surfaces covered with multi-layer isolation. This includes all boom and body panels except for the two solar arrays. For earth albedo and infrared emission, a polynomial/harmonic approximation of measured values from the Clouds and Earth's Radiant Energy System (CERES) is used that describes the dominant latitudinal and seasonal variations. Earth radiation pressure contributions from individual surface elements in the visible part of the Earth are summed using a ring-zone approach with 22 segments similar to Knocke et al. (1988). Atmospheric drag and lift-forces are computed using Sentman's formulation for the composition-dependent accommodation coefficients (Doornbos 2012) and summed over all plates of the macro-model. Atmospheric density values and chemical composition data are obtained from the NRLMISE-00 model of Picone et al. (2002). Similar to the cannon-ball model, a global scale factor is estimated for solar radiation pressure and atmospheric forces to compensate for possible errors in

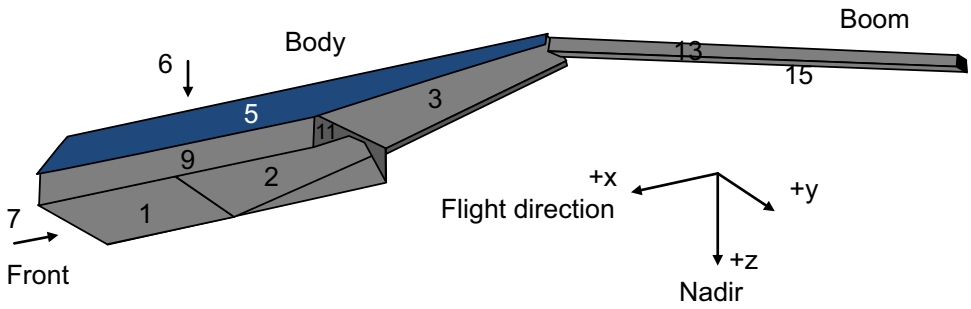


**Fig. 2** Schematic view of the Swarm satellite and the plates of the macro-model

**Table 2** Swarm macro-model

| # | Panel | Normal vector | Area ($m^2$) | $\alpha_{vis}$ | $\delta_{vis}$ | $\rho_{vis}$ | $\alpha_{IR}$ | $\delta_{IR}$ | $\rho_{IR}$ |
|---|---|---|---|---|---|---|---|---|---|
| 1 | Bottom 1 | (+0.000, +0.000, +1.000) | 1.54 | 0.18 | 0.79 | 0.03 | 0.68 | 0.31 | 0.01 |
| 2 | Bottom 2 | (−0.198, +0.000, +0.980) | 1.40 | 0.77 | 0.17 | 0.06 | 0.78 | 0.20 | 0.02 |
| 3 | Bottom 3 | (−0.138, +0.000, +0.990) | 1.60 | 0.86 | 0.14 | 0.00 | 0.78 | 0.22 | 0.00 |
| 4 | Solar array right | (+0.000, +0.588, −0.809) | 3.45 | 0.90 | 0.10 | 0.00 | 0.72 | 0.28 | 0.00 |
| 5 | Solar array left | (+0.000, −0.588, −0.809) | 3.45 | 0.90 | 0.10 | 0.00 | 0.72 | 0.28 | 0.00 |
| 6 | Top | (+0.000, +0.000, −1.000) | 0.50 | 0.93 | 0.07 | 0.00 | 0.78 | 0.22 | 0.00 |
| 7 | Front | (+1.000, +0.000, +0.000) | 0.56 | 0.20 | 0.80 | 0.00 | 0.17 | 0.83 | 0.00 |
| 8 | Side wall $+y$ | (+0.000, +1.000, +0.000) | 0.75 | 0.90 | 0.07 | 0.03 | 0.78 | 0.21 | 0.01 |
| 9 | Side wall $-y$ | (+0.000, −1.000, +0.000) | 0.75 | 0.90 | 0.07 | 0.03 | 0.78 | 0.21 | 0.01 |
| 10 | Support front | (+1.000, +0.000, +0.000) | 0.80 | 0.45 | 0.00 | 0.55 | 0.80 | 0.00 | 0.20 |
| 11 | Support back | (−1.000, +0.000, +0.000) | 0.80 | 0.93 | 0.07 | 0.00 | 0.78 | 0.22 | 0.00 |
| 12 | Boom $+y$ | (+0.000, +1.000, +0.000) | 0.60 | 0.64 | 0.03 | 0.33 | 0.79 | 0.09 | 0.12 |
| 13 | Boom $-y$ | (+0.000, −1.000, +0.000) | 0.60 | 0.64 | 0.03 | 0.33 | 0.79 | 0.09 | 0.12 |
| 14 | Boom top | (−0.239, +0.000, −0.971) | 0.60 | 0.83 | 0.06 | 0.11 | 0.78 | 0.18 | 0.04 |
| 15 | Boom bottom | (+0.228, +0.000, +0.974) | 0.60 | 0.45 | 0.00 | 0.55 | 0.80 | 0.00 | 0.20 |

For each panel the surface area and normal vector in the spacecraft body frame are given along with the optical properties in the visual (vis) and infrared (IR) spectral range

the adopted plate sizes and optical properties of the macro-model. For earth radiation pressure (ERP), in contrast, a fixed scale factor of one is adopted. Adjustment of a free ERP scale factor is essentially equivalent to estimating an unconstrained empirical radial acceleration and would allow errors in the knowledge of the radial GNSS antenna offset from the center-of-mass to propagate into a corresponding shift of the estimated orbit.

The complementary roles of a priori models for the non-gravitational forces and the estimation of empirical accelerations in the POD of low earth orbit satellites have earlier been discussed in Hackel et al. (2017) for the TerraSAR-X spacecraft, which orbits in a similar altitude as the highest Swarm satellite, but maintains a sun-synchronous dusk-dawn orbit at all times. Since processing standards for Swarm PSOs and reprocessed orbits differ in multiple aspects, dedicated tests based on 1 year (2016) of Swarm-C data have been conducted to isolate the impact of refined non-gravitational force modeling using macro-models on precise orbit determination for this mission. As an immediate effect, consideration of earth radiation pressure in the force modeling changes the mean orbital radius for the observed period of revolution by 3–5 mm and thus results in a slightly different vertical leveling of the orbit. Furthermore, systematic horizontal orbit offsets that result from the correlation of SRP accelerations and cross-track position for high elevations of the sun above the orbit plane can be reduced when using the macro-model. Such offsets can be evidenced in a direct comparison of POD solutions using cannon-ball SRP and drag models and can independently be inferred from the analysis of SLR observations. For Swarm, these errors were found to exhibit amplitudes of about 1 cm in float-ambiguity POD solutions. Finally, a small reduction in the standard deviation of the estimated empirical accelerations (5–10%) can be observed, when replacing the cannon-ball models for solar radiation pressure and atmospheric forces by the more sophisticated macro-models. However, it is not possible to renounce the estimation of empirical accelerations even when using the refined macro-models due to the lacking predictability of atmospheric density. On the other hand, consideration of the refined non-gravitational force models in the orbit determination process is expected to assist proper

calibration of the Swarm accelerometers as well as atmospheric density retrieval.

For single-receiver ambiguity fixing, observations are first grouped into passes of continued carrier phase tracking and the mean value of the Hatch–Melbourne–Wübbena (HMW) combination (Leick et al. 2015) for each pass is determined from the dual-frequency code and phase observations. Upon correction with the satellite-specific wide-lane biases provided as part of the GRG product, between-passes differences of the HMW combination—and thus the wide-lane biases—can be fixed to integer values. Making use of these values and the float-valued ambiguity estimates of the ionosphere-free carrier phase combination for each pass obtained with GRG clock offsets values, the inter-pass differences of the L1 ambiguity can subsequently be determined and constrained to integer values. Details of this concept and the GHOST-specific implementation are described in Laurichesse et al. (2009) and Montenbruck et al. (2017).

Over the 4-year time frame covered by the present analysis, 95th percentile fixing rates of 97.9% for wide-lane ambiguities and 93.9% for L1 (narrow-lane) ambiguities were achieved for Swarm-C using acceptance criteria of 0.4 and 0.2 cy, respectively (Fig. 3). Notable variations of the L1 fixing rates in 2014 are attributed to pronounced seasonal variations of the ionospheric scintillation activity and the resulting tracking quality in this time frame. An obvious drop in the success-rate for wide-lane ambiguity fixing can be recognized between May 6, 2015 and May 4, 2016 due to a temporary doubling of the delay locked loop (DLL) bandwidth for semi-codeless P(Y)-code tracking. This resulted in a 40% increase of the code noise (from about 0.8–1.1 m for the ionosphere-free L1/L2 combination) and an associated change in the standard deviation of the wide-lane ambiguity (approx. 0.08–0.12 cy). Less pronounced variations in the wide-lane success-rate can also be recognized following a two-step increase in the field of view (FoV) in Dec. 2014/Jan. 2015. Since May 2016, stable ambiguity fixing rates of 99.1 and 96.5% are achieved on Swarm-C for the wide-lane and L1 ambiguity, respectively. Similar values are obtained for the other two spacecraft of the Swarm constellation.

Complementary to the reduced dynamic orbit determination discussed so far, kinematic position solutions based on ambiguity-fixed carrier phase observation have been computed in the reprocessing for the first time to support gravity field analyses within the Swarm project (Jäggi et al. 2016; da Encarnação et al. 2016). Traditionally, kinematic orbit determination involves the estimation of epoch wise positions and clock offsets as well as float-valued ambiguities of the ionosphere-free carrier phase observations for each pass (van den IJssel 2015; Montenbruck 2003). Making use of the resolved inter-pass differences of wide-lane and L1 ambiguities determined in the reduced dynamic orbit determination, it is now possible to also incorporate the corresponding ambiguity constraints into the kinematic orbit determination. The resulting solutions exhibit a notably increased geometric stability compared to their float-ambiguity counterpart, but remain purely kinematic in nature, since no explicit use is made of the dynamical model information.

For proper modeling of the carrier phase observations, wave-front distortions of the antenna caused by static multipath and the near-field antenna environment need to be compensated through a corresponding antenna pattern in the observation modeling. Empirical phase patterns for the ionosphere-free L1/L2 carrier phase combination consistent with the new processing standard have, therefore, been estimated for this work using a residuals stacking approach (Jäggi et al. 2009b) and subsequently employed in both the reduced dynamic and kinematic processing. The patterns are based on 36 days of observations (day of year DOY 10, 20, …, 360) covering the full year 2016 with diverse sun aspect angles with respect to the orbital plane. A total of three iterations were performed and contributions of the

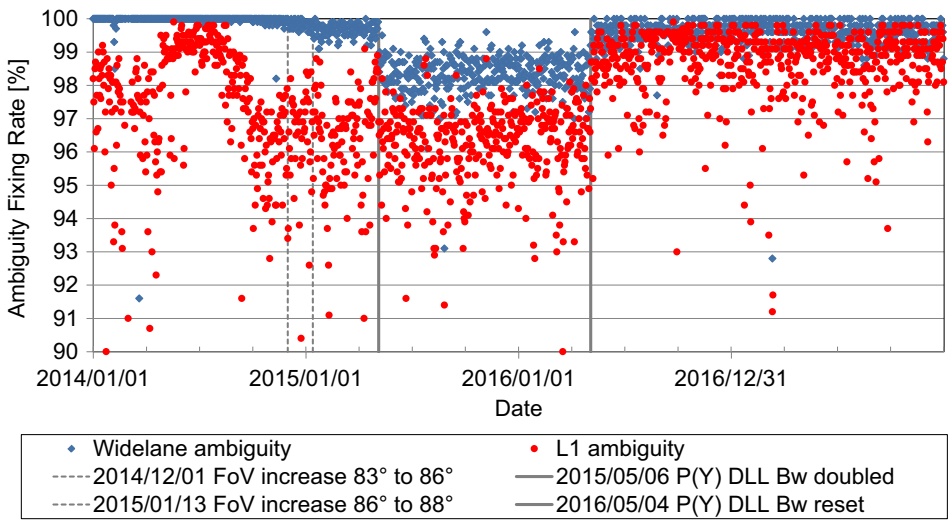


**Fig. 3** Fraction of passes with resolved wide-lane and L1 ambiguities for the Swarm-C satellite. Major variations in the ambiguity success-rate relate to changes in the receiver configuration

final iteration to the estimated pattern amount to roughly 1 mm RMS. Compared to float-ambiguity solutions, convergence in the estimated phase pattern and the resulting orbits is achieved with a lower number of iterations (2–3 vs. 5 or more). Daily average cross-track offsets between orbits computed with and without phase pattern correction amount to less than 1 mm. This is different from findings reported in van den IJssel et al. (2015), where seasonally varying cross track biases of up to 2 cm amplitude were identified in a similar comparison. The absence of such biases in the present processing can be attributed to the benefit of a refined solar radiation pressure model as well as the stabilizing effect of carrier phase ambiguity fixing for the precise orbit determination of the Swarm satellites.

Phase variations of the three individual satellites (Swarm-A, -B,- C) are strikingly similar (Fig. 4), which evidences a very small scatter in the manufacturing of the spacecraft and antennas. Overall the patterns closely resemble those reported in van den IJssel et al. (2015), but benefit from modified mask angles in the receivers and now cover boresight angles of up to 88° on all three spacecraft. Pronounced fringes with amplitudes of 10–20 mm may be recognized that can be attributed to diffraction or reflection of signals by structural elements in the vicinity of the antenna. These effects are incompletely covered by multipath simulation and anechoic calibrations of the GPS antennas conducted prior to the Swarm mission (Wettergren et al. 2009), and the manufacturer supplied patterns have, therefore, been discarded in favor of the inflight calibrations for the Swarm precise orbit determination. Making use of the calibrated phase patterns, daily averages of the carrier phase residuals ranging from 5 to 7 mm RMS are obtained in the reprocessing. Peak values apply for receiver configurations with a narrow phase locked loop (PLL) bandwidths and periods of strong scintillation (van den IJssel et al. 2016). Following the latest receiver configuration changes in the mid of 2016, stable residuals of about 5.4 mm RMS are achieved on the Swarm-A/C pair and an even slightly better value (4.9 mm RMS) on their higher-altitude sibling, Swarm-B.

## Performance assessment

Based on the processing standards described above, a new version of Swarm precise science orbits has been generated covering the period since initial operation (late Nov. 2013) to end of 2017. Within this section, the performance of the reprocessed orbits is assessed and compared with that of the past release of Swarm PSOs. Distinct analyses are provided for reduced dynamic and kinematic solutions.

### Reduced dynamic orbits

For assessment of the Swarm POD performance, the Swarm PSOs and the newly computed orbits are compared against satellite laser ranging (SLR) measurements. Other than ephemeris overlap or inter-agency comparisons (Tapley et al. 2004; Peter et al. 2017), SLR represents a completely independent space-geodetic measurement technique and can thus be used to evaluate not only the precision (repeatability), but also the accuracy of GPS-based orbit products for low earth orbit (LEO) satellites.

All three Swarm satellites are routinely tracked by a worldwide network of SLR observatories under the coordination of the International Laser Ranging Service (ILRS; Pearlman et al. 2002). Over the 4 years since launch, roughly half a million normal points have been collected for the Swarm mission, where each normal point represents a 5 s average of individual high-rate ranging measurements. Roughly half of all normal points result from tracking of the Swarm-B satellite. The remainder is shared among the Swarm-A and -C satellites, which always exhibit common station visibilities due to their moderate separation (Table 3).

SLR residuals, i.e., differences of measured and modeled ranges, constitute a well-established means for validating the

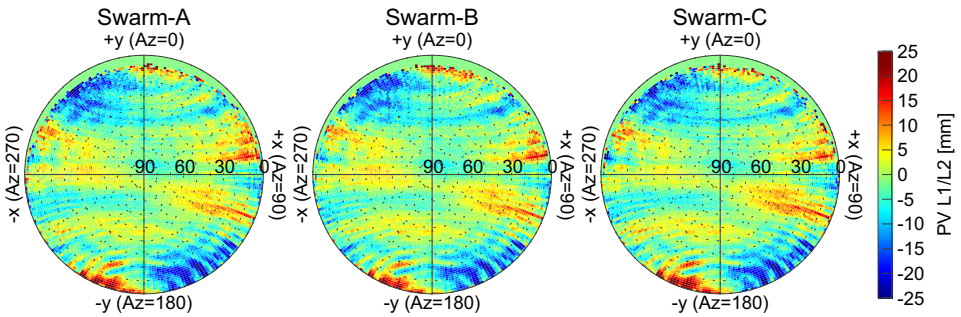


**Fig. 4** Phase variations of the ionosphere-free L1/L2 carrier phase combination for the primary GPS antennas of Swarm-A, -B, -C relative to the nominal phase center. The center of the polar plot corresponds to the boresight direction of the antenna, which is nominally aligned with the zenith direction. The *y*-axis of the antenna system is aligned with the forward-pointing +*x*-body axis

**Table 3** Number of SLR normal points for the Swarm satellites collected since start of the mission (Nov. 2013) up to the end of 2017

| Satellite | Total | Selected stations | Accepted |
|---|---|---|---|
| Swarm-A | 111,678 | 89,138 | 87,015 |
| Swarm-B | 307,270 | 253,590 | 247,262 |
| Swarm-C | 110,276 | 89,903 | 87,566 |

Individual columns provide the amount of observations obtained by all stations in the ILRS network, the selected subset of 14 high-performance stations and the number of normal points accepted after data screening

accuracy of GPS-based precise orbit determination for LEO satellites (Arnold et al. 2018). In the first instance, the analysis of SLR observations provides a statistical measure of the one-dimensional range difference, from which an estimate of the total position error can be obtained. Beyond that, SLR residuals can also be used to infer systematic orbit errors of the LEO satellite and/or corrections to the SLR site coordinates and ranging biases. Such corrections are vital to fully exploit the SLR measurement performance, but partly limit the capability to identify systematic orbit errors. In particular, vertical station position errors cannot be distinguished from radial orbit errors.

For the present work, a subset of 14 ILRS stations was selected, for which the SLR residuals (including measurement errors and orbit errors) of the reprocessed orbits exhibit a representative standard deviation of 10 mm or better. Using the full 4-year data set and all three Swarm satellites, corrections of the SLRF2014 station coordinates and range biases were estimated from the SLR residuals of the reprocessed orbits. For the selected stations, SLRF2014 position corrections of up to 15 mm and range bias corrections up to 28 mm were obtained in good overall agreement with results of Arnold et al. (2018) based on different LEO satellites and a 1-year time frame. Consideration of these corrections provides a reduction of the RMS SLR residuals from 13 to 11 mm and from 10 to 8 mm, for the precise science orbits and the reprocessed orbits, respectively. In all computations, a 10° elevation mask and a 99.74th percentile outlier screening threshold were applied.

As illustrated by Table 4, the SLR residuals of reprocessed orbits exhibit a notably smaller standard deviation. On average over the full set of analyzed stations and satellites, a 30% reduction is achieved (Fig. 5). The benefit is most pronounced for high-performance laser stations such as Graz, Herstmonceux, Matera, and Zimmerwald, which offer a very low normal point scatter and stable station calibrations. Here, reductions of about 40% are obtained, and the resulting SLR residuals indicate orbit errors down to the 5 mm (1D) level.

Compared to the reprocessed orbits, a mean value of − 1.4 mm can be noted in the PSO SLR residuals. This corresponds to a mean radial orbit difference of about 3 mm between the two solutions and can be attributed to the neglect of earth radiation pressure in the PSO processing. Comparing the individual Swarm satellites, small-satellite-specific deviations (of about 1–2 mm) from the constellation mean may be noted in the SLR residuals, which show up in a similar way for the PSO and reprocessed orbits. These biases can be attributed to inconsistencies of about 3 mm in the assumed radial center-of-mass (CoM) offsets of the

**Table 4** SLR residuals of Swarm reduced dynamic precise science orbit and reprocessed orbits for 14 high-performance stations after application of station-specific position and range bias corrections

| Station | PSO | | | Reprocessing | | |
|---|---|---|---|---|---|---|
| | Swarm-A | Swarm-B | Swarm-C | Swarm-A | Swarm-B | Swarm-C |
| Graz | −0.7 ± 10.2 | −3.6 ± 9.8 | −0.7 ± 10.8 | 1.5 ± 6.8 | −0.7 ± 6.5 | 1.2 ± 6.3 |
| Greenbelt | −0.7 ± 11.9 | −2.9 ± 11.3 | −1.8 ± 11.5 | 1.1 ± 8.3 | −0.8 ± 8.2 | −0.8 ± 8.5 |
| Haleakala | 0.5 ± 10.6 | −2.3 ± 10.5 | −3.0 ± 13.1 | 1.1 ± 8.3 | −0.2 ± 8.2 | −1.6 ± 9.7 |
| Hartebeesthoek | 0.4 ± 11.6 | −1.8 ± 11.8 | −0.4 ± 12.2 | 1.6 ± 9.8 | −0.7 ± 8.7 | 0.1 ± 10.2 |
| Herstmonceux | −0.7 ± 10.6 | −3.4 ± 10.1 | −2.9 ± 10.5 | 1.4 ± 6.0 | −0.4 ± 5.7 | 0.2 ± 6.5 |
| Matera | −0.9 ± 8.8 | −3.9 ± 9.9 | 3.4 ± 8.5 | 1.4 ± 4.8 | −0.9 ± 5.4 | 2.4 ± 4.4 |
| Monument Peak | 0.5 ± 11.1 | −1.3 ± 11.4 | −1.3 ± 11.7 | 1.1 ± 8.0 | −0.4 ± 8.2 | −0.4 ± 8.4 |
| Mount Stromlo | 2.2 ± 11.4 | −0.4 ± 10.6 | 0.9 ± 10.4 | 1.5 ± 7.0 | −0.5 ± 6.6 | 1.0 ± 8.2 |
| Papeete | 1.1 ± 11.0 | −3.2 ± 9.4 | −0.6 ± 12.0 | 1.4 ± 11.5 | −0.8 ± 8.7 | 0.7 ± 8.7 |
| Potsdam | −0.5 ± 11.1 | −4.3 ± 10.7 | −2.3 ± 11.5 | 1.6 ± 7.3 | −0.7 ± 7.0 | 0.9 ± 8.7 |
| Wettzell (SOSW) | 1.9 ± 12.7 | −5.9 ± 11.7 | 0.3 ± 11.2 | 0.4 ± 8.1 | −0.9 ± 8.1 | 5.5 ± 8.0 |
| Wettzell (WLRS) | −0.3 ± 12.2 | −3.8 ± 12.9 | −2.7 ± 13.8 | 1.5 ± 7.3 | −0.5 ± 8.4 | 0.4 ± 9.5 |
| Yarragadee | 0.9 ± 11.0 | −1.1 ± 10.3 | −0.3 ± 10.6 | 1.1 ± 8.1 | −0.8 ± 7.4 | 0.6 ± 8.0 |
| Zimmerwald | −0.6 ± 10.5 | −3.3 ± 11.0 | −2.9 ± 10.7 | 1.7 ± 7.1 | −0.4 ± 6.8 | 0.1 ± 7.3 |
| Total | 0.4 ± 11.1 | −2.1 ± 10.8 | −1.0 ± 11.1 | 1.2 ± 7.9 | −0.6 ± 7.4 | 0.5 ± 8.1 |
| Total (all satellites) | | | −1.4 ± 10.9 | | | 0.0 ± 7.7 |

Each entry gives the mean value ± standard deviation in units of millimeter

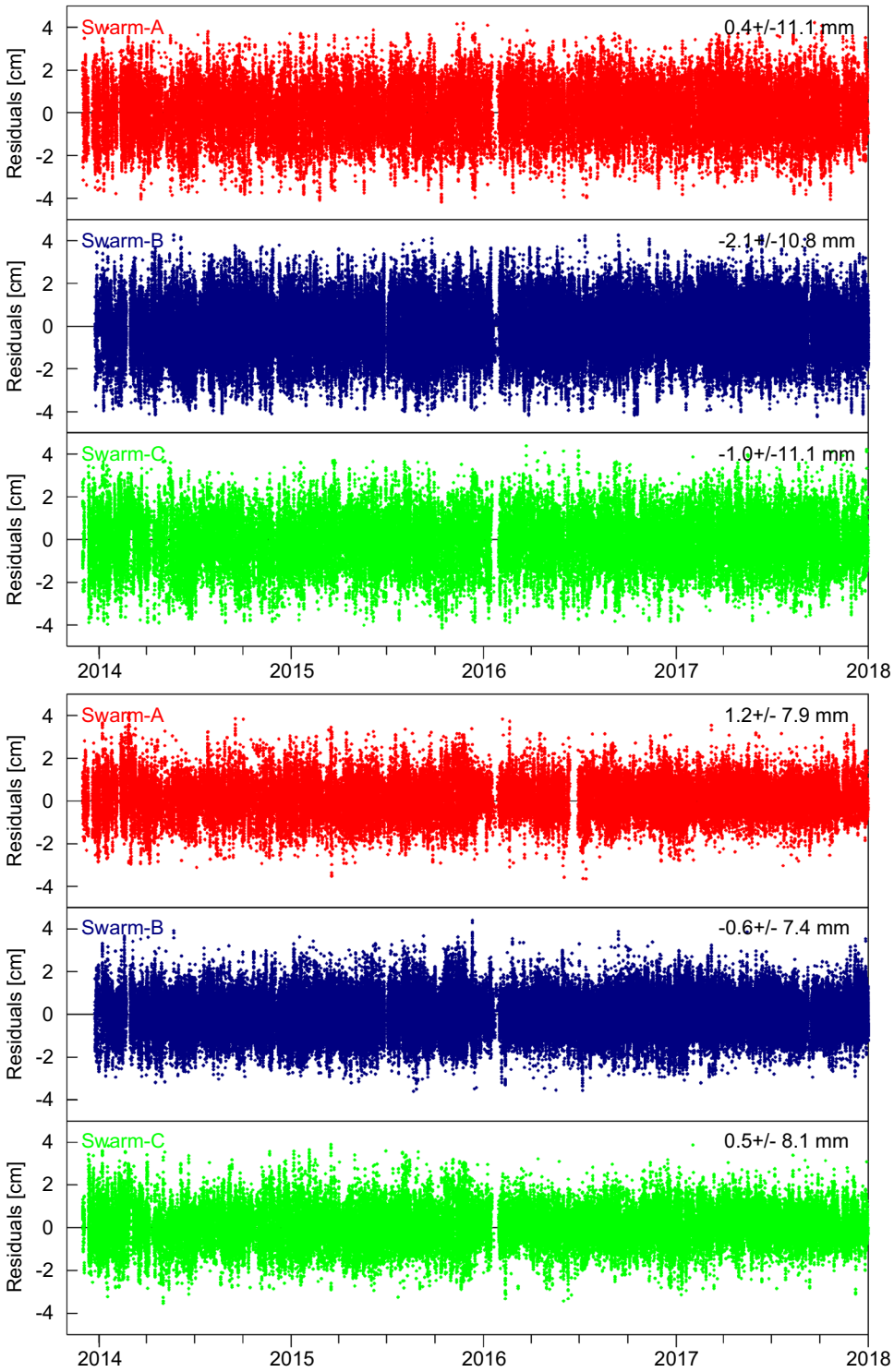


**Fig. 5** SLR residuals of Swarm precise science orbits (top) and reprocessed orbits (bottom) after application of station position and range bias corrections. Numbers in the top right corner of each subplot indicate the mean value ± standard deviation of the residuals over the entire time frame and all satellites. The SLR data gap in January 2016 is related to a limited availability of predicted Swarm orbits for ILRS station operations over a 2 weeks period

laser retroreflector (LRR) reference points for the various satellites and indicate the precision, with which the mass distribution in the fuel tanks and the resulting overall center-of-mass position can be predicted for a given spacecraft design.

Over the 4-year period, a gradual improvement of the overall orbit determination quality can be noted for both PSOs and reprocessed orbits. RMS SLR residuals for the PSOs decrease from roughly 12 mm in 2014 to 10 mm in 2016 and 2017, while the reprocessed orbits show a reduction from about 9–7 mm. This performance improvement is largely related to refined settings of the carrier phase tracking loops for semi-codeless P(Y) code tracking that were

**Table 5** SLR residuals statistics of Swarm-C orbits for 2016 obtained with different model options and using the same stations and station coordinate/bias corrections as in Table 4

| Non-gravitational force model | Ambiguities | Residuals |
|---|---|---|
| Cannon-ball (drag, SRP) | Float | −2.2 ± 11.6 |
| Macro-model (drag/lift, SRP, ERP) | Float | 0.1 ± 10.8 |
| Cannon-ball (drag, SRP) | Fixed | −1.9 ± 7.9 |
| Macro-model (drag/lift, SRP, ERP) | Fixed | −0.0 ± 7.9 |

Results are gives as mean value ± standard deviation in units of millimeter

implemented in the course of 2015 (van den IJssel et al. 2016) as well as an overall decrease of ionospheric activity within the time frame of interest.

While the comparison of SLR residuals clearly demonstrates the improved quality of the reprocessed orbits, it is not immediately obvious to what extent individual changes in the processing standards contribute to this improvement. To further analyze this aspect, separate sets of Swarm-C orbits covering 1 year were computed, in which different options for the handling of non-gravitational forces and the carrier phase ambiguities were used. The resulting SLR residual statistics are summarized in Table 5.

As expected, the largest residuals are obtained for the basic solution with cannon-ball model and float ambiguity estimation that is representative of the PSO processing approach. Introduction of the refined macro-modeling results in only a slight reduction of the standard deviation. I addition, a small shift in the mean value can be noticed, which reflect the lowering of the orbit caused by consideration or earth radiation pressure in the orbit determination process. The ambiguity fixing, in contrast, enables an almost 30% reduction of the standard deviation irrespective of the non-gravitational force modeling. It clearly outperforms the contribution of the macro-modeling and is mainly responsible for the performance improvement in the present reprocessing.

## Kinematic orbits

Next to the reduced dynamic orbits, carrier phase based kinematic position solutions were computed as part of both the PSO product and the reprocessing. Due to the absence of dynamical constraints, the kinematic solutions are generally of inferior quality than the reduced dynamic counterpart, which can readily be recognized from a direct comparison of kinematic and reduced dynamic orbit solutions, but likewise shows up in the respective SLR residuals.

For the PSO product, differences between kinematic and reduced dynamic orbits amount to roughly 3.5 cm (median of daily RMS position difference) over the 4-year analysis period. This is 2–3 times lower than reported in van den IJssel et al. (2015) for the first year of the Swarm mission and again reflects the receiver performance improvements and reduced ionospheric activity for the subsequent years. For the reprocessed Swarm POD products, the median of the daily RMS differences between kinematic and reduced dynamic orbits amounts to only 1.7 cm, which clearly demonstrates the benefit of ambiguity fixing for the kinematic positioning. The performance gain is most pronounced up to mid-2015, where the float ambiguity solution suffers most from the tracking problems caused by narrow tracking loops and high scintillation activity. This results in kinematic position errors of about 8 cm (median of daily 3D RMS) in that period, while the reprocessed solution is found to be substantially more robust with corresponding errors below 2.5 cm.

SLR residuals for the reprocessed solutions are summarized in Table 6. The selected stations, screening limits and site corrections match those previously described for the analysis of the reduced dynamic orbits. Again, a substantial (factor-of-two) improvement can be noted for the new ambiguity-fixed solutions compared to the earlier float-ambiguity processing. While short-term noise in the kinematic solutions is mainly driven by the carrier-phase noise and GPS satellite clock errors and is thus comparable in both types of solutions, the float ambiguity processing provides a reduced geometric stiffness and may induce systematic errors over orbital time scales along with sudden discontinuities in case of interrupted tracking. Ambiguity fixing, in contrast, provides a notably smoother variation of the position errors as shown for a sample day in Fig. 6.

To characterize the smoothness of the kinematic position solutions over different time scales in a quantitative manner, we consider the Allan deviation of the position error relative to the reprocessed reduced dynamic reference orbit, which describes the standard deviation of the mean velocity error over specified time intervals. While originally developed for the characterization of oscillator stability (Allan 1987; Riley 2008), it can likewise be used for a statistical assessment of orbit errors and their correlations over time as suggested by Jäggi et al. (2009a).

Results for a sample 1-day data arc are shown in Fig. 7. For the reprocessed product, the Allan deviation of the

**Table 6** SLR residuals of Swarm kinematic precise science orbit and reprocessed orbits

| Satellite | PSO | Reprocessing |
|---|---|---|
| Swarm-A | +0.4 ± 19.5 | +0.1 ± 10.2 |
| Swarm-B | −2.2 ± 21.5 | −1.7 ± 9.4 |
| Swarm-C | −1.0 ± 23.0 | −0.6 ± 10.5 |

Each entry gives the mean value ± standard deviation in units of millimeter

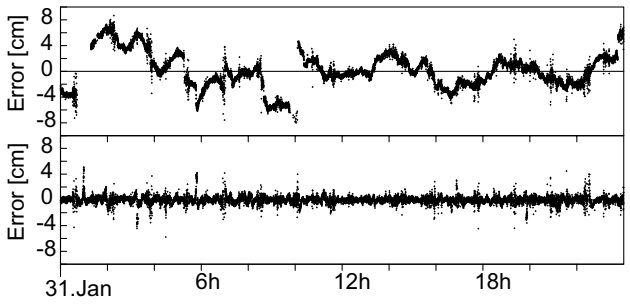


**Fig. 6** Crosstrack errors of kinematic Swarm-C positions for Jan 31, 2016 based on comparison with an ambiguity-fixed reduced dynamic reference orbit. Top: precise science orbit product; bottom: reprocessed orbits

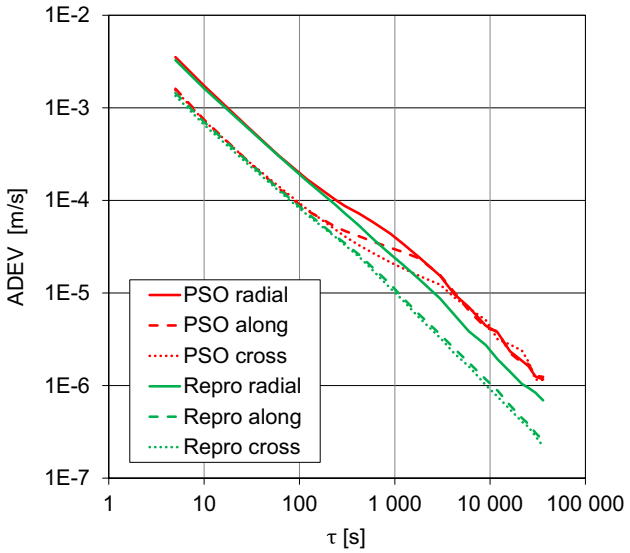


**Fig. 7** Allan deviation of Swarm-C position errors in radial (solid), along-track (dashed), and cross-track (dotted) direction for PSO (red) and reprocessed (green) kinematic position solutions on Jan 31, 2016

kinematic position errors exhibits a linear variation with slope −1 in the double-logarithmic representation over time scales of $\tau = 5$ s to $\tau = 10$ h for all components. This is representative of uncorrelated (white noise) with standard deviations of about 6 mm in the horizontal (along-track and cross-track) and 14 mm in the vertical (radial) direction. Similar characteristics apply for the PSO product up to time scales of 100 s, whereas a factor of 2–3 increase of the Allan deviation can be observed above 15 min. Errors at this time scale would affect the determination of low degree and order (typically 2–6) gravity field coefficients. The quality of the reprocessed kinematic orbits thus suggests a high potential for improved Swarm-only gravity field solutions in this domain. Further studies will be required, though, to assess whether this potential benefit can be materialized in view of other problems (e.g., the separation of non-gravitational acceleration in the absence of high-performance accelerometers) affecting the gravity field analysis in this mission.

## Summary and conclusions

A new and improved set of Swarm precise science orbits has been generated from observations of the onboard GPS receivers using refined processing concepts. Key changes include the use of a macro-model for enhanced non-gravitational force modeling and the use of carrier phase ambiguity fixing, which has become possible after correction of half-cycle ambiguities in the raw GPS measurements.

Only a limited benefit of the refined macro-modeling can be noted in the reduced dynamic orbit solution, which still requires substantial empirical accelerations to compensate force modeling deficiencies at the low altitude. On the other hand, both the reduced dynamic and kinematic orbit solutions show a notable improvement as a result of the carrier phase ambiguity fixing. Overall a 30% reduction of orbit errors in the reduced dynamic orbits can be inferred from the analysis of satellite laser ranging measurement. With errors of about 0.5–1 cm in each axis, the new ambiguity-fixed Swarm solution can contribute to the calibration of SLR station coordinates and range biases as well as the independent validation of the SLR–GPS frame tie.

For the kinematic orbits, a 50% overall performance improvement is achieved, and orbit errors relative to a reduced dynamic solution show white noise characteristics over extended time scales. This marks a major improvement over the past release of kinematic precise science orbits that suffer from increased errors at time scales of 15 min and up. The improved kinematic solutions may thus contribute to refining Swarm gravity field solutions at low degree and order.

## References

Allan DW (1987) Time and frequency (time-domain) characterization, estimation, and prediction of precision clocks and oscillators. IEEE Trans Ultrason Ferroelectr Freq Control 34(6):647–654

Arnold D, Montenbruck O, Hackel S, Sosnica K (2018) Satellite laser ranging to low Earth orbiters: orbit and network validation. J Geodesy. https://doi.org/10.1007/s00190-017-1090-2

Bock H, Dach R, Jäggi A, Beutler G (2009) High-rate GPS clock corrections from CODE: support of 1 Hz applications. J Geodesy 83(11):1083–1094. https://doi.org/10.1007/s00190-009-0326-1

Cerri L, Berthias J, Bertiger W, Haines B, Lemoine F, Mercier F, Ries J, Willis P, Zelensky N, Ziebart M (2010) Precision orbit determination standards for the Jason series of altimeter missions. Mar Geodesy 33(S1):379–418. https://doi.org/10.1080/01490419.2010.488966

da Encarnação JT, Arnold D, Bezděk A, Dahle C, Doornbos E, IJssel J, Jäggi A, Mayer-Gürr T, Sebera J, Visser P, Zehentner N (2016)

Gravity field models derived from Swarm GPS data. Earth Planets Space 68(1):127. https://doi.org/10.1186/s40623-016-0499-9
Dach R, Schaer S, Arnold D, Prange L, Sidorov D, Susnik A, Villiger A, Jaeggi A (2017). CODE final product series for the IGS. Astronomical Institute, University of Bern, Bern. http://www.aiub.unibe.ch/download/CODE. https://doi.org/10.7892/boris.75876.2
Dahle C, Arnold D, Jäggi A (2017) Impact of tracking loop settings of the Swarm GPS receiver on gravity field recovery. Adv Space Res 59(12):2843–2854. https://doi.org/10.1016/j.asr.2017.03.003
Doornbos E (2012) Thermospheric density and wind determination from satellite dynamics. Springer, Heidelberg
Friis-Christensen E, Lühr H, Knudsen D, Haagmans R (2008) Swarm—an Earth observation mission investigating geospace. Adv Space Res 41(1):210–216. https://doi.org/10.1016/j.asr.2006.10.008
Hackel S, Montenbruck O, Steigenberger P, Balss U, Gisinger C, Eineder M (2017) Model improvements and validation of TerraSAR-X precise orbit determination. J Geodesy 91(5):547–562
Jäggi A, Beutler G, Prange L, Dach R, Mervart L (2009a) Assessment of GPS-only observables for gravity field recovery from GRACE. In: Sideris MG (eds) Observing our changing Earth. Springer, Berlin, pp 113–123
Jäggi A, Dach R, Montenbruck O, Hugentobler U, Bock H, Beutler G (2009b) Phase center modeling for LEO GPS receiver antennas and its impact on precise orbit determination. J Geodesy 83(12):1145–1162. https://doi.org/10.1007/s00190-009-0333-2
Jäggi A, Dahle C, Arnold D, Bock H, Meyer U, Beutler G, van den IJssel J (2016) Swarm kinematic orbits and gravity fields from 18 months of GPS data. Adv Space Res 57(1):218–233
Johnston G, Riddell A, Hausler G (2017) The international GNSS service. In: Teunissen P, Montenbruck O (eds) Springer handbook of global navigation satellite systems. Springer, Berlin, pp 967–982
Knocke PC, Ries JC, Tapley BD (1988) Earth radiation pressure effects on satellites. In: AIAA/AAS astrodynamics conference, pp 577–587
Laurichesse D, Mercier F, Berthias JP, Broca P, Cerri L (2009) Integer ambiguity resolution on undifferenced GPS phase measurements and its application to PPP and satellite precise orbit determination. Navigation 56(2):135–149. https://doi.org/10.1002/j.2161-4296.2009.tb01750.x
Leick A, Rapoport L, Tatarnikov D (2015). GPS satellite surveying. Wiley, Hoboken
Loyer S, Perosanz F, Mercier F, Capdeville H, Marty JC (2012) Zero-difference GPS ambiguity resolution at CNES-CLS IGS analysis center. J Geodesy 86(11):991. https://doi.org/10.1007/s00190-012-0559-2
Montenbruck O (2003) Kinematic GPS positioning of LEO satellites using ionosphere-free single frequency measurements. Aerosp Sci Technol 7(5):396–405. https://doi.org/10.1016/S1270-9638(03)00034-8
Montenbruck O, Hackel S, Jäggi A (2017) Precise orbit determination of the Sentinel-3A altimetry satellite using ambiguity-fixed GPS carrier phase observations. J Geodesy. https://doi.org/10.1007/s00190-017-1090-2
Olsen N, Finlay CC, Kotsiaros S, Tøffner-Clausen L (2016) A model of Earth's magnetic field derived from 2 years of Swarm satellite constellation data. Earth Planets Space 68(1):124. https://doi.org/10.1186/s40623-016-0488-z
Pearlman MR, Degnan JJ, Bosworth JM (2002) The international laser ranging service. Adv Space Res 30(2):135–143. https://doi.org/10.1016/S0273-1177(02)00277-6
Peter H, Jäggi A, Fernández J, Escobar D, Ayuga F, Arnold D, Wermuth M, Hackel S, Otten M, Simons W, Visser P, Hugentobler U, Féménias P (2017) Sentinel-1A—first precise orbit determination results. Adv Space Res 60(5):879–892. https://doi.org/10.1016/j.asr.2017.05.034
Picone JM, Hedin AE, Drob DP, Aikin AC (2002) NRLMSISE-00 empirical model of the atmosphere: statistical comparisons and scientific issues. J Geophys Res. https://doi.org/10.1029/2002JA009430
Riley WR (2008) Handbook of frequency stability analysis, NIST Special Publication 1065. National Institute of Standards and Technology, Boulder,
Sieg D, Diekmann F (2016) Options for the further orbit evolution of the Swarm mission. In: Proceedings of living planet symposium, SP-740, p 278
Siemes C, da Encarnação JDT, Doornbos E, van den IJssel J, Kraus J, Pereštý R, Grunwaldt L, Apelbaum G, Flury J, Olsen PEH (2016) Swarm accelerometer data processing from raw accelerations to thermospheric neutral densities. Earth Planets Space 68(1):92. https://doi.org/10.1186/s40623-016-0474-5
Tapley B, Schutz B, Born GH (2004) Statistical orbit determination. Academic Press, London
van den IJssel J, Encarnação J, Doornbos E, Visser P (2015) Precise science orbits for the Swarm satellite constellation. Adv Space Res 56(6):1042–1055
van den IJssel J, Forte B, Montenbruck O (2016) Impact of Swarm GPS receiver updates on POD performance. Earth Planets Space 68(1):85
Wermuth M, Montenbruck O, van Helleputte T (2010) GPS high precision orbit determination software tools (GHOST). In: 4th International conference on astrodynamics tools and techniques, 3–6 May 2010, Madrid
Wettergren J, Bonnedal M, Ingvarson P, Wästberg B (2009) Antenna for precise orbit determination. Acta Astronaut 65(11–12):1765–1771
Zangerl F, Griesauer F, Sust M, Montenbruck O, Buchert B, Garcia A (2014) SWARM GPS precise orbit determination receiver initial in-orbit performance evaluation. In: Proceedings of ION GNSS + 2014, pp 1459–1468

**Oliver Montenbruck** is head of the GNSS Technology and Navigation Group at DLR's German Space Operations Center. His research activities comprise spaceborne GNSS receiver technology, autonomous navigation systems, spacecraft formation flying and precise orbit determination as well as new constellations and multi-GNSS processing. Oliver Montenbruck presently chairs the Multi-GNSS Working Group of the International GNSS Service and coordinates the performance of the MGEX Multi-GNSS Experiment.

**Stefan Hackel** is a flight dynamics engineer at DLR's German Space Operations Center. He received his M.Sc. degree from Munich's University of Technology in 2012 and is currently doing his PhD in precise orbit determination of low earth spacecraft, where he works on refined dynamical model, integer ambiguity fixing of GPS observations, and external orbit validation methods.

**Jose Ijssel** is a senior researcher in the Astrodynamics & Space Missions section of the faculty of aerospace engineering at TU Delft. Her research focusses on precise orbit determination of LEO satellites with applications to gravity field analysis and thermospheric density retrieval.

**Daniel Arnold** is a senior researcher at the Astronomical Institute of the University of Bern. He is responsible for LEO orbit and gravity field determination at AIUB and in charge of the routine processing of GNSS orbits and clocks for the CODE analysis center. Since January 2016 he is the head of the satellite geodesy subgroup LEO orbit and gravity field determination.